Journal of Directed Energy, **2**, Summer 2006, 5–21

Modeling of Laser Charring and Material Removal in Fiberglass Materials

Vladimir V. Semak

Electro-Optics Center, Pennsylvania State University, P.O. Box 30, State College, Pennsylvania 16804

and

Timothy F. Miller*

Applied Research Laboratory, Pennsylvania State University, P.O. Box 30, State College, Pennsylvania 16804

A numerical model of the physical processes governing laser charring of fiberglass materials has been developed. The model is three-dimensional and transient and incorporates submodels for volumetric and surface laser energy absorption, pyrolysis chemistry kinetics, pyrolitic gas outfluxing, char removal via chemical reaction, and radar attenuation resulting from char formation. This model differs from previous char modeling work because it deals with volumetric, in addition to surface, energy absorption. Modeling results are compared directly with measurements of temperature, char thickness, and optical and radar transmission made on fiberglass material test slabs in a wind tunnel. The comparisons show very good agreement and illustrate subtle behaviors associated with changes in heat transfer and char thickness. Because of uncertainties in important physical properties, some empirical input of thermophysical properties to the model is necessary. However, the amount of this empirical input is manageable and enables close prediction over a large range of laser flux.

KEYWORDS: Charring, Fiberglass, High-energy laser, Modeling

Nomenclature

A	surface absorptivity
A_i	reaction preexponential constant
a, b	empirical wind-tunnel coefficients
c	specific heat
f	volume fraction
H	enthalpy
h	heat transfer coefficient
I	irradiance
K	thermal conductivity
k	Boltzmann's constant

Received August 23, 2005; revision received May 31, 2006.
*Corresponding author; e-mail: nfn@psu.edu.

M	Mach number of external flow
M_a	molecular weight
m	mass flux
N_a	Avogadro number
n	number density of char centers
np	empirical wind-tunnel exponent
q	heat flux
R	radar intensity
r_p	char particle radius
s	surface area
T	temperature
t	time
V	volume
Δ	specimen thickness
ε	surface emissivity
μ	absorption coefficient
ν	kinetics rate
ρ	density
σ	Stefan–Boltzmann constant

1. Introduction

The set of the main physical and chemical processes accompanying laser interaction is specific and large for a given type of material. It is possible to construct a generic model of laser interaction that incorporates all currently known science related to the laser interaction; however, either the simulation will be impossible or its accuracy will be low due to the computational problems associated with the complex code corresponding to the complex physical model. Therefore, in order to perform a high-accuracy simulation of laser-induced charring a physical model was constructed that included only main physical and chemical phenomena governing the laser interaction with fiberglass composite materials. Numerous computational experiments and verification exercises against extensive experimental data were performed to perfect the suite of selected physical–chemical phenomena. A particular goal was to minimize the number of these adjustable parameters.

Although physical/computational models for char-forming materials have been proposed and exercised previously,[1,5,9,10,13,17] the present work differs from and expands upon the prior work in several significant ways. Prior work deals almost exclusively with the formation and subsequent ablation of char during reentry or hypersonic flight. In these cases heating is through the surface (which is the location of the char initiation site as well) while, depending on laser wavelength, heat generation and char formation can occur volumetrically. Even with surface laser absorption, the temperatures that occur are substantially lower than those seen during reentry. Consequently ablation or other surface removal processes are different. In this work, new treatments of char pyrolysis kinetics and thermomechanical effects specific to composite materials are introduced. Finally, results from this treatment are compared directly with measurements[11†] of optical transmission, surface temperature, char thickness, and radar frequency (RF) attenuation.

†Although Ref. 11 may not be readily available to some researchers, the author of Ref. 11 anticipates releasing a publicly available reference in the form of an Applied Research Laboratory/Penn State University Research Memorandum.

2. Physical Description

The physical and computational models were developed to simulate laser interaction with a fiberglass composite material that consists of glass fiber layers woven with layers of epoxy in between. The epoxy wets the fiberglass layers and after solidification keeps the fiberglass layers together. In our model, the weave patterns and the orientation of the fiberglass sheets are the important parameters that affect the heat transfer and charring initiation and kinetics.

The physical model developed for the laser-induced charring of fiberglass requires specific attributes:

- Volumetric absorption of the laser beam in the material (and subsequent heating)
- Surface cooling due to the effect of the airflow, thermal radiation, and the surface evaporation of glass
- Multistep thermal decomposition of the epoxy with production of gas and final production of char
- Growth of the char particles nucleated in the voids of the fiberglass weave pattern and evaporation of these char particles
- Fracturing of the glass fibers and, related to that, surface erosion
- Attenuation of radar radiation by the char particles produced in the material.

The laser beam is absorbed by both the fiberglass material and the char particles. The laser beam absorption in fiberglass is wavelength dependent. For the wavelength of a Nd:YAG laser, 1.06 μm, the absorption length in fiberglass is comparable to (or exceeds) the target thickness (i.e., >1 cm). Although the laser beam absorption length at 1.06 μm is different for fiberglass and for epoxy, the fiberglass composite was considered as a homogeneous material and an average absorption length was used. Experiments[11] demonstrated that absorption length in the fiberglass material for the radiation of a Nd:YAG laser increases with the increase of the material temperature. The physical properties of the fiberglass material studied here were density of 2,000 kg/m^3, specific heat of 1,044 J/kg-K, heat conductivity at room temperature of 0.4 W/m-K, and latent heat of evaporation in the range from 7 to 13 MJ/kg. (Typically a 10-MJ/kg value was used in the calculations here.) Although thermal decomposition or melting of epoxy might result in the change of its optical properties, the possibility was not modeled here. For the case of CO_2 lasers, it is well known that organic materials, such as epoxy, and silicon-based glass are strongly absorbing at wavelengths in the far infrared.[2,3] Therefore we assumed that the beam of a CO_2 laser is absorbed at relatively short length, very much smaller than the thickness of the target, such that the absorption can be considered as occurring entirely at the surface.

The absorption of both wavelengths by char particles occurs in a very short distance, very much smaller than the characteristic diameter of a char particle. The size of the char particles increases starting from zero. Thus, initially the size of the particles can be much smaller than or comparable to the absorption length. However, measurements of Nd:YAG laser and radar transmission demonstrate that the growth of char particles is so rapid that the stage when particles are transparent to the optical radiation need not be modeled.

Refraction in the glass fibers and density fluctuations of the epoxy cause laser beam scattering. We have performed numerical experiments in order to study the effect of scattering on the spatial distribution of the laser irradiance in the material and the related spatial distribution of the heating rate. The laser beam scattering was modeled on a macroscopic level by using scattering coefficients representing an average description of the scattering.

The results demonstrated a negligible effect of scattering on the thermal field. Although not specifically addressed here, modeling on the microscopic level can reveal local hot areas produced by refraction and scattering in the inhomogeneous material. These hot areas have a potential role in char nucleation.

Absorbed laser radiation causes an increase of material temperature. Absorbed laser irradiance can be spatially nonuniform or Gaussian-like (especially if from nonlaboratory sources), which also causes nonuniformity of the thermal field. Note, though, that the shape of the laser profile does not affect the subsequent theoretical development. The coefficients of heat conductivity of glass and epoxy are different. Therefore, the heat conductivity of a composite material consisting of layers of fiberglass with layers of epoxy is anisotropic: coefficients of heat conductivity along the fiberglass layers and in the direction perpendicular to the fiberglass layers are different. Although anisotropic conductivity models can be developed, the model in the present work used an average heat conductivity disregarding its anisotropy. The laser beam is larger than the characteristic length of the heat conduction along the fiberglass layer. Therefore, disregarding the anisotropy introduces a negligible error in the computation of the thermal field.

3. Mathematical Model of Laser-Induced Charring

3.1. Thermal field

The thermal field in the target is computed according to Eq. (1):

$$c\rho\frac{\partial T(z,t)}{\partial t} = \nabla\{K[T(z,t)]\nabla T(z,t)\} + q_{\text{laser}}(z,t) - q_{\text{ph}}(z,t), \tag{1}$$

where c is the specific heat of material, ρ is the density, K is the temperature-dependent heat conductivity, q_{laser} is the heat source due to absorption of laser radiation, and q_{ph} is the heat sink due to phase transformation (polymer breakdown).

At elevated temperatures, epoxy decomposes and produces gas. The gas products can accumulate between the fiberglass layers. When the pressure of gas exceeds the material strength, delamination can occur that results in a significant (orders of magnitude) decrease of heat conductivity. This effect is also taken into account by the model. The authors propose that the temperature dependence of the heat conductivity of uncharred composite material, reflecting the delamination effect, is given by Eqs. (2):

$$\begin{aligned} &K(T) = K_1, \quad \text{for} \quad T < T_1, \\ &K(T) = K_1 - (K_1 - K_2) \times [T(z,r) - T_1]/(T_2 - T_1), \quad \text{for} \quad T_1 < T < T_2, \\ &K(T) = K_2, \quad \text{for} \quad T > T_2, \end{aligned} \tag{2}$$

with $T_1 = 700$ K and $T_2 = 1{,}200$ K. The linear dependence of the thermal conductivity of the virgin fiberglass was required to reproduce specific behavior in the temperature and optical absorption measurements.[11] This topic is discussed at greater length in the discussion section. The coefficient of heat conductivity of charring material is

$$K_\Sigma = K(1 - f_{\text{char}}) + K_{\text{char}} f_{\text{char}}, \tag{3}$$

where f_{char} is the volumetric fraction of charred material and K_{char} is the heat conductivity of char. The coefficients used in the numerical simulation of laser charring of the fiberglass composite studied here were $K_1 = 0.4$ W/mK, $K_2 = 0.05$ W/mK, and $K_{\text{char}} = 6.0$ W/mK. The value for K_1 is consistent with that advocated in Ref. 17 for virgin silica/phenolic,

whereas K_{char} is consistent with the value advocated in Ref. 7 for char. The reduced value for K_2 is consistent with the effect of delamination and the formation of gas space and is consistent with the values used in Ref. 5.

The heat source due to the absorption of laser radiation, q_{laser}, in Eq. (1) is expressed by the equation

$$q_{\text{laser}}(z, t) = \mu_\Sigma(z) I(z, t), \tag{4}$$

where μ_Σ is the absorption coefficient and I is the laser beam irradiance at the location with coordinate z along the z axis, which is normal (always in the present work, though the theoretical development is not impacted by the assumption of oblique irradiation) to the target surface and directed along the laser beam propagation. The beam intensity is expressed by the Beer–Lambert law

$$I(z, t) = A I_0(t) \exp\left[-\int_0^z \mu_\Sigma(z, t)\, \mathrm{d}z\right], \tag{5}$$

where A is the surface absorptivity and I_0 is the incident beam irradiance.

Radar attenuation measurements offer another means of model validation. The attenuation of the radar radiation by the char particles is modeled assuming Beer–Lambert attenuation inside an individual particle. The coefficient of absorption is related directly to the char electric conductivity. Experimental measurements[6] have demonstrated that the char, formed as a result of thermal decomposition of epoxy, is electrically conductive if its temperature exceeds approximately 1,070 K. The atomic structure of graphite changes from amorphous to crystalline near this temperature, allowing it to conduct electricity and, therefore, absorb RF radiation. It is worth noting that some workers[4] found that the structure of pure graphite transitioned around 1,600 K, while others[18] found that "hydrogenated" carbon transitioned at 523 K. Our model gave the best matching with the experimental data if the char particles were assumed to be nonconductive and transparent to the radar radiation, when during formation the char temperature remained below 1,150 K.

We assume that the char particles are opaque to the laser radiation. The char particles are small such that the diffraction averages the laser intensity at the distance much smaller than the sample thickness; i.e., the diffraction geometry for an individual particle corresponds to the far-field case. The thickness of the sample is small relative to the distance at which beam divergence due to scattering on the char particles must be taken into account; i.e., the scattering geometry for the particle ensemble corresponds to the near-field case. Hence the attenuation of average laser intensity I can be described in terms of geometric shadowing:

$$\frac{\mathrm{d}I}{\mathrm{d}z} = -I \pi r_p^2 n, \tag{6}$$

where r_p is the radius of the char particle and n is the number density of the char particles. Then the absorption coefficient μ can be expressed in terms of char particle radius r_p and particle number density n:

$$\mu = \pi r_p^2 n. \tag{7}$$

The relation between the char particle radius r_p, particle number density n, and volumetric fraction of the char f_{char}, is given by the equation

$$\tfrac{4}{3} \pi r_p^3 n = f_{\text{char}}. \tag{8}$$

The absorption coefficient μ can be expressed in terms of volumetric fraction of char f_{char} and number density of char particles n:

$$\mu = \sqrt[3]{\left(\tfrac{9}{16}\pi f_{\text{char}}^2 n\right)}. \tag{9}$$

The coefficient of absorption of the material is given by the equation

$$\mu_\Sigma(z,t) = \mu[T(z,t)] + \left\{\tfrac{9}{16}\pi f_{\text{char}}^2[T(z,t)]n\right\}^{1/3}. \tag{10}$$

The first term on the right-hand side of Eq. (10) is the absorption coefficient of uncharred material. Comparison with experimental measurements, after the fact, demonstrated that the temperature dependence of the uncharred material can be approximately expressed as

$$\begin{aligned}
&\mu(T) = \mu_0, && \text{for} \quad T < T_{T1},\\
&\mu(T) = \mu_0 - (\mu_0 - \mu_1) \times [T(z,r) - T_{T1}]/(T_{T2} - T_{T1}), && \text{for} \quad T_{T1} < T < T_{T2},\\
&\mu(T) = \mu_1, && \text{for} \quad T > T_{T2}.
\end{aligned} \tag{11}$$

The coefficients have the values $\mu_0 = 360\ \text{m}^{-1}$, $\mu_1 = 200\ \text{m}^{-1}$, $T_{T1} = 380$ K, and $T_{T2} = 520$ K. The second term on the right-hand side of Eq. (10) describes optical attenuation by the char particles. The linear dependence was required to enable prediction of the observed[11] trend of increasing transmission with increased temperature prior to the onset of char formation.

The boundary condition expressing heat fluxes at the target surface is given by the equation

$$I_{\text{surf}} = -K[T(0,t)]\frac{\partial T(0,t)}{\partial z} + \frac{\mathrm{d}}{\mathrm{d}s}\left(\frac{\partial m_{\text{ev}}}{\partial t}\right) H_{\text{ev}} + [h_{\text{conv}}(t) + h_{\text{radiation}}(t)][T(0,t) - T_f], \tag{12}$$

where $\partial m_{\text{ev}}/\partial t$ is the surface evaporation rate, $\mathrm{d}s$ is the surface area element, H_{ev} is the latent heat of evaporation of the surface material, h is the coefficient of convective heat exchange, $T(0,t)$ is the surface temperature, and T_f is the recovery temperature of the airflow. The heat transfer coefficient incorporates the effective radiation heat transfer coefficient ($h_{\text{radiation}} = \sigma\varepsilon[T(0,t)^2 + T_f^2][T(0,t) + T_f]$).

Four processes affect the heat exchange at the target surface: convective heat exchange with the external airflow, thermal radiation from the surface, degassing from the surface due to the epoxy chemical decomposition, and evaporation of the glass near the surface. The specimens modeled here were charred in a subsonic wind tunnel under both stagnant conditions and with $M = 0.9$ airflow.[11] Convective cooling was modeled using Newton's cooling law (i.e., cooling at the surface is proportional to the difference of temperature of the surface and the recovery temperature of the airflow). The temporal behavior of the convective heat exchange coefficient h is shown schematically in Fig. 1. The initial slow reduction of h is approximated by the equation $h = a/(t+b)^{np}$. The coefficients a, b, and np and the time of evaporation onset are established empirically and are based on the specific characteristics of the test wind tunnel. In the experimental studies,[11] the laser was turned on after a delay relative to the turning on of the wind tunnel. The time delay corresponds to the period during which airflow establishes and velocity reaches a steady-state value. Detailed measurements of surface heat transfer were made in the portable blow-down wind tunnel used for testing.[11] The time dependence of the heat exchange coefficient was computed for the specific conditions of the experiment, i.e., flow velocity, wind-tunnel geometry, and pressure in the gas cylinders, and this submodel was developed to ensure proper correlation

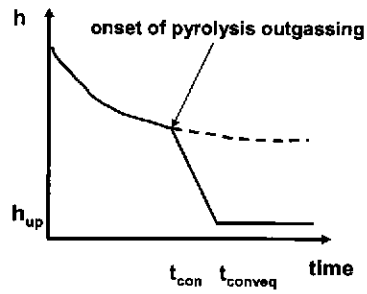

Fig. 1. Transient convective heat transfer behavior.

with the experiment. The degassing from the surface affects the heat flow at the target surface. The flow of the gaseous products of epoxy decomposition produces a blanketing effect, preventing the heat exchange between the ambient airflow and the target surface. This phenomenon is described in more detail in Refs. 8 and 14.

The surface evaporation produces cooling at elevated temperatures. We believe that for the case of the fiberglass composite material, the evaporation of glass is responsible for the stabilization of the surface temperature observed experimentally. The cooling effect of evaporation is strongly dependent on the latent heat of evaporation. The values of the latent heat of evaporation from solid glass and from molten glass are different. Therefore, the temperature dependence of the evaporation-related surface cooling is different for solid and for molten glass. This difference is accounted for in the model.

Radiation heat flux was modeled simply as $\varepsilon\sigma(T^4_{\text{surface}} - T^4_{\text{ambient}})$. The emissivity ε is taken to be ~0.9 (consistent with other sources[1,5,9,13,17]). For an ambient temperature of 20°C, the radiant heat fluxes for surface temperatures of 1,000, 1,500, and 2,000°C are 13, 50, and 136 W/cm^2, respectively. Radiation heat transfer had an insignificant effect during the initial heating of the specimen. At the higher temperatures, after charring has started, it can be a significant fraction of the laser flux (especially in the context of diminished convective cooling once charring begins).

3.2. Chemical reaction

The last term on the right-hand side of heat transfer equation (1) describes the heat sink due to polymer breakdown, and subsequent char formation. Assuming a three-stage reaction of the breakdown, the heat sink is given by the equation

$$q_{\text{ph}}(z,t) = \frac{\partial f_1(z,t)}{\partial t}\rho_1 H_1 + \frac{\partial f_2(z,t)}{\partial t}\rho_2 H_2 + \frac{\partial f_3(z,t)}{\partial t}\rho_3 H_3, \tag{13}$$

where f_1, f_2, and f_3 are the fractions of the reaction components; ρ_1, ρ_2, and ρ_3 are the densities of the reaction components; and H_1, H_2, and H_3 are the enthalpies of the reaction stages. The reasoning pertaining to the selection of three stages is described below.

The production of char was modeled as a growth of the char particles that nucleate in the gaps of the weave pattern of the fiberglass layers. The rate of the particle growth is defined by the rate of the charring reaction. The growth of the char particles occurs as a result of temperature increase. The char particle growth is countered by the removal rate from the char particle surface by chemical reaction or mechanical removal. The reaction rate increases with the temperature increase. The char particle size can be stabilized at a

certain level and then starts decreasing when all fuel for the char formation is depleted or the temperature is increased to high values such that the removal rate is higher than the char formation rate.

The process of epoxy charring is a result of thermal decomposition of the polymer molecules. Detailed information on the chemical reactions of thermal decomposition of epoxy is unavailable. Although multistage (specifically "three-stage") charring kinetics have been proposed,[1,5,13,17] we have rejected the form used by these references as inadequate. In these references the overall kinetics rate equals the sum of several (usually three) separate Arrhenius-type expressions; each is dominant over a limited temperature range. However, when one considers the temperature range of laser-induced charring, essentially only one of the expressions is used; the others contributed insignificantly. For all intents and purposes, these models function as single-step models.

The attempt is made with the three-stage mechanism proposed here to accommodate the sequential reaction mechanisms described by Torre et al.,[15] who suggest that initial reactions occur at lower temperatures (up to ~600°C), with further heating of the exposed surface at elevated temperatures (up to ~1,800°C) producing char. This view suggests that a polymer-cracking reaction may be a more appropriate model. During the first stage the polymer molecules break, releasing volatile products. The shorter polymer molecules produced at the first stage of the reaction break into even shorter molecules during the second stage, producing additional volatile products. Finally, at the third stage the short molecules break again, generating char and volatile products. The reaction rates are temperature dependent, and the charring proceeds faster as material temperature increases due to laser beam absorption. The parameters of the three-stage reaction of epoxy charring, i.e., the rate constants and activation energies, are determined by matching numerically predicted rates of char production with the experimentally measured rates.

A three-stage chemical reaction responsible for the epoxy breakdown and charring is given by the system of equations

$$\frac{\partial V_0}{\partial t} = -v_1 V_0 - v_{g1} V_0, \tag{14a}$$

$$\frac{\partial V_1}{\partial t} = v_1 V_0 - v_2 V_1 - v_{g2} V_1, \tag{14b}$$

$$\frac{\partial V_2}{\partial t} = v_2 V_1 - v_3 V_2 - v_{g3} V_2, \tag{14c}$$

$$\frac{\partial V_3}{\partial t} = v_3 V_2, \tag{14d}$$

where V_0 is the volume of the epoxy material, V_1 and V_2 are the volumes of the intermediate products, V_3 is the volume of char, and the reaction rates are denoted by the letter v with index corresponding to the stage number and gaseous products (denoted by the subscript g). The volumetric fraction of char is $f_{\text{char}} = V_3/V_0$. Equations (14a)–(14d) describe a cascade-like effect. The loss of virgin material, V_0, during the first stage [Eq. (14a)] is dependent on the amount of virgin material present at the time (i.e., if no material exists, then no material can be removed). Some of this loss is in the form of gaseous products, and some goes to form material 1. We assume that there is no catalysis due to the presence of other materials. The amount of material 1 [Eq. (14b)] increases as material is transformed from the virgin state and reduces as material 1 is lost to the gas phase or to the formation of material 2. This sequence is repeated until the char formation stage [Eq. (14d)].

Table 1. Specific reaction kinetics coefficients for sample fiberglass

Reaction stage (i)	A_i, 1/s	H_i, MJ/kg	A_{gi}, 1/s	H_{gi}, MJ/kg
1	800	0.8	900	0.9
2	1,200	0.93	900	0.9
3	500	1.0	0	0.9

The reaction rates corresponding to ith stage are given by the equation

$$v_i = A_i \exp\left[-\frac{M_{a,i} H_i}{N_a k T(z,t)}\right], \tag{15}$$

where A_i is the reaction constant, $M_{a,i}$ is the molecular weight of the ith component, H_i is the enthalpy of the ith reaction, N_a is the Avogadro number, and k is Boltzmann's constant. The specific kinetic terms that best fit the fiberglass data compared here are listed in Table 1. These values were determined by matching the predicted onset and rate of increase of RF attenuation with measurements[11] and are appropriate for fiberglass materials similar to those studied here. These values produce good agreement over a large flux and convective cooling range.

3.3. Char removal/radar attenuation

The attenuation of the radar intensity is given by the equation

$$\frac{\mathrm{d}R(z,t)}{\mathrm{d}z} = R(z,t)\left\{\left[1 - \exp\left(-\mu_{\mathrm{ch}}^{r} 2r_p\right)\right]\pi r_p^2 n\right\}, \tag{16}$$

where μ_{ch}^{r} is the attenuation of radar radiation in the char, n is the number density of char particles, and r_p is the char particle radius related to the volumetric fraction of char f_{char} by the equation

$$r_p = \left(\frac{3}{4}\frac{f_{\mathrm{char}}}{\pi n}\right)^{1/3}. \tag{17}$$

The growth of the char particle radius r_p can be determined using the volumetric fraction of char $f_{\mathrm{char}}(t)$, which is changing in time as described by the three-stage chemical reaction of thermal decomposition of polymer epoxy. Here μ_{ch}^{r} is equal to zero for temperatures less than 1,150 K to account for the transparency of amorphous char to RF radiation. For temperatures in excess of 1,150 K, $\mu_{\mathrm{ch}}^{r} = 10^8$ m^{-1} for the specimen char. The number density of char particles is related directly to the number of nucleation sites, and that was assumed to be proportional to the glass fiber weave density. For best agreement n equaled 10^{12} sites/m^3.

Surface char is subject to removal by the action of a number of mechanisms: chemical reaction, erosion (due to impinging matter), and aerodynamic shear-induced erosion. Scala[12] describes the mass-transfer regimes associated with ablating graphite (assuming no mechanical erosion). The reaction rate controlled through diffusion-rate-controlled regimes can be modeled using one- and two-film theory (as described by Turns[16]). With the one-film model, carbon is assumed to react kinetically with oxygen to create carbon dioxide. (The oxygen must still diffuse through a boundary layer of reaction products and inert species.) At sufficiently high surface temperatures the oxygen near the surface is depleted and the

reaction mechanism transforms to the two-film model. With this model, carbon reacts with carbon dioxide away from the surface to produce carbon monoxide that subsequently reacts with the atmospheric oxygen. At higher temperatures, the reaction rate is solely dominated by the rate at which oxidizer can diffuse to the reaction zone. Note that this diffusion rate can be augmented substantially in a convective flow environment. Our initial diffusion-limited predictions agreed well with the theoretical limit determined by Scala.[12] These preliminary calculations also suggest that surface chemical reactions at the temperatures of interest during laser-induced charring were not sufficient to produce the level of removal observed during testing. Measurements of char surface regression rates in this work indicate rates roughly an order of magnitude greater than those observed experimentally.[11] An additional mechanism, structural failure of the char,[13] was implemented initially; however, due to lack of knowledge about the mechanical properties of both virgin and charred material, it was not used for the present work.

The chemical removal rate is modeled here as a decrease of the char particle size due to reaction with, or erosion by, volatiles produced by char formation in the specimen:

$$\frac{\partial r_p}{\partial t} = A_C \exp\left[-\frac{M_{aC} H_C}{N_a k T(z,t)}\right], \tag{18}$$

where A_C is the reaction constant for carbon, M_{aC} is the molecular weight of carbon, H_C is the heat of reaction, N_a is the Avogadro number, k is the Boltzmann constant, and $T(z,t)$ is the local temperature at the moment of time t. Note that the difference between this formulation and the too-low chemical reaction described earlier is that it centers on the interaction of the internal char particles with the volatile flow. The very large specific area of the small char particles relative to a monotonic sheet of graphite produces substantially elevated reaction and removal rates.

4. Numerical Model

The block diagram of the numerical algorithm for the self-consistent solution of the system of Eqs. (1)–(13) is shown in Fig. 2. The input data for the computations are as follows:

1. Initial temperature of material $T_0(z, r)$
2. Laser beam intensity distribution at the surface $I_0(r, t)$
3. Material density ρ and specific heat c
4. Parameters for material heat conductivity, K_1, K_2, T_1, T_2[‡]
5. Char density ρ_{ch}, specific heat c_{ch}, and heat conductivity K_{ch}
6. Char atomic mass M_A, latent heats of phase transformations H_i and $H_{i,g}$[‡]
7. Constants of charring reaction A_i and $A_{i,g}$[‡]
8. Parameters for absorption coefficient of material, μ_0, μ_1, T_{T1}, T_{T2}[‡] [see Eq. (11)]
9. Material absorptivity at the laser wavelength A_{char}, absorption coefficient for radar wavelength μ_{ch}^r[‡]
10. Convective heat transfer coefficients h_{f1}, h_{f2}
11. Flow equilibrium time t_0, power of time dependence $h(t)$, n_p
12. Evaporation reduction of convective cooling, t_{conv}, t_{conveq}, h_{up}
13. Time step δt, integration time t_{int}
14. Material thickness Δ

[‡]Parameters requiring empirical input.

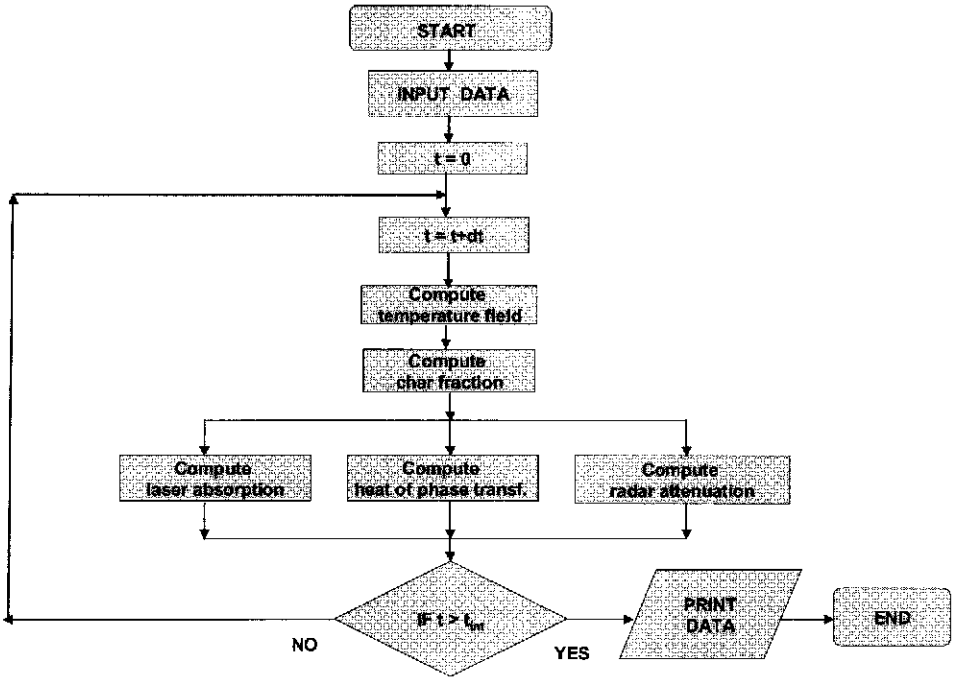

Fig. 2. Flowchart of computation sequence.

Initially, the number of empirically based parameters appears daunting. However, it is the authors' contention that the number of significant parameters is reasonably small, given the problem complexity. Obviously, such input data as the initial sample temperature, sample thickness, and beam intensity and distribution are at the discretion of the user. Flow characteristics must be obtained by characterization or modeling of the wind-tunnel or other environment for which the simulations are made. Thermophysical properties such as specific heat and density are deemed not to change much from values available from the literature. The thermal conductivity and absorptivity of the virgin material can be obtained by a comparison to a few sets of stagnant-flow measurements of optical transmission and surface temperature, with no knowledge of char kinetics required. The latent heats can be obtained from inspection of the locations of inflections in the prechar temperature profile. The kinetics of the charring reactions can be obtained by comparison of the onset times of char formation. A process of parameter estimation for other materials is unavoidable. The values proposed in this work are specific to a particular fiberglass. Therefore each new material should be evaluated separately. However, we believe that the procedure described here for determining them makes the process less onerous.

The output of the code includes a three-dimensional temperature field, a three-dimensional distribution of char volumetric fraction (including material loss), the time-dependent optical transmissivity of the sample integrated over the laser beam, the time-dependent radar attenuation, and the time-dependent surface temperature in the center of the laser beam. The governing transient differential energy equation was implicitly discretized using the finite volume method into a collection of coupled algebraic equations. The discretization had second-order spatial and first-order temporal accuracy. Although

three-dimensional calculations are possible, the calculations made here were two-dimensional (r and z) to reduce computational time. A grid consisting of 50 radial and 50 axial volumes was sufficient to produce a grid-independent solution. A time step of 1 ms was used as well. Theoretically the implicit backward differencing of the time derivative is unconditionally stable. However, the thermophysical and kinetic properties were evaluated from the previous time iteration, so care was taken that the time step was small enough to guarantee time-step-independent results.

5. Model Verification

5.1. Optical transmission

Measurements[11] of optical transmission of Nd:YAG radiation through fiberglass composite material were used to determine the empirical thermal conductivity and optical absorption coefficients. Figures 3a–3d show comparisons between measured transmission and predictions made using the coefficients listed earlier for samples of different thicknesses and for different fluxes. These were not cooled by convective airflow. The empirical coefficients were determined by simultaneously matching the maximum value of transmission, the time that the maximum occurs, and the shape of the curves. It is significant to note that a single set

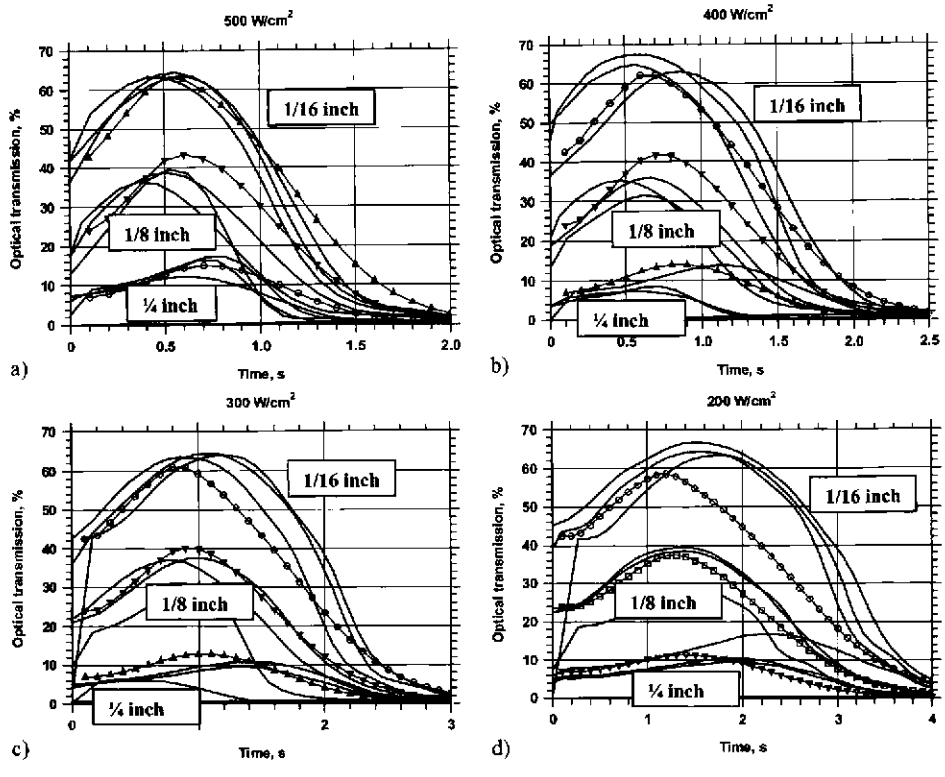

Fig. 3. Computed (symbols and lines) and measured[11] (lines) optical transmission for fiberglass for Nd:YAG laser interaction for different power fluxes and specimen thicknesses under no-airflow conditions.

of constants produces such good agreement over a large range of incident flux and specimen thickness.

The tendency for increasing transmission with increasing temperature (or time) has been noted earlier. The point where transmission begins to fall off corresponds to the onset of char formation. The experimental data also showed an interesting tendency to delay the location of peak transmission for thinner materials. It was this observation that necessitated the relationship for thermal conductivity that was shown earlier, which we attributed to delamination effects.

5.2. Surface temperature and RF attenuation

The computed and measured data[11] presented below are for both a Nd:YAG laser and a CO_2 laser. The material of the target was a composite fiberglass, the thickness of the target was 0.63 cm, the specimen radii were 4 cm, the laser spot radii were 2.54 cm for 175 and 300 W/cm^2 and 1.85 cm for 500 W/cm^2, and the radar beam radius was 1.25 cm. The predicted surface temperature and radar attenuation for Nd:YAG laser irradiance of 175 W/cm^2 are shown in Fig. 4. These and all remaining calculations simulated irradiation in the presence of a $M = 0.9$ airflow parallel to the specimen surface. The surface temperature predictions agree reasonably well with measurements. The various curves represent separate test runs under the same conditions. The radar attenuation, however, differs substantially from the measurements. The predicted radar attenuation increases initially to a value approximately four times higher than the measured value and then decreases to a value that is approximately two times higher than the measured attenuation. In all situations, the low-power data exhibited the greatest variance, perhaps due to of the greater influence of cooling losses. At lower power levels the amount of outgassing from the specimen is reduced; consequently the convective insulating effect due to the outgassing (as illustrated in Fig. 1) is much reduced as well. Higher power levels yielded much more repeatable measurements.

The predicted temperatures and radar attenuations for the Nd:YAG laser irradiances of 300 and 500 W/cm^2, shown in Figs. 5 and 6, differ from the measured data by less than 10%, which is less than the statistical variation of the measurements. The predicted

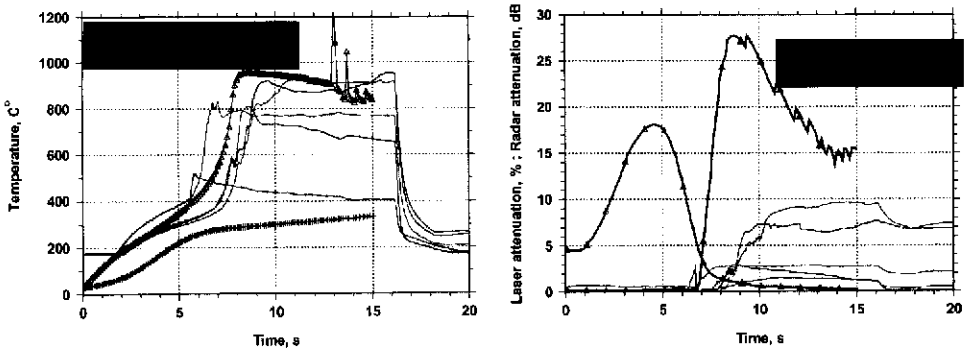

Fig. 4. Computed (symbols and lines) and measured[11] (lines) surface temperature and radar transmission for fiberglass for Nd:YAG laser (175 W/cm^2) interaction in airflow $M = 0.9$ with surface outgassing.

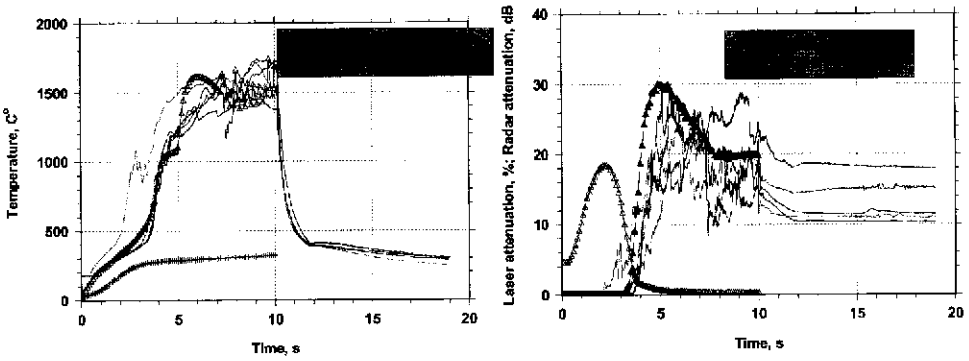

Fig. 5. Computed (symbols and lines) and measured[11] (lines) surface temperature and radar transmission for fiberglass for Nd:YAG laser (300 W/cm^2) interaction in airflow $M = 0.9$ with surface outgassing.

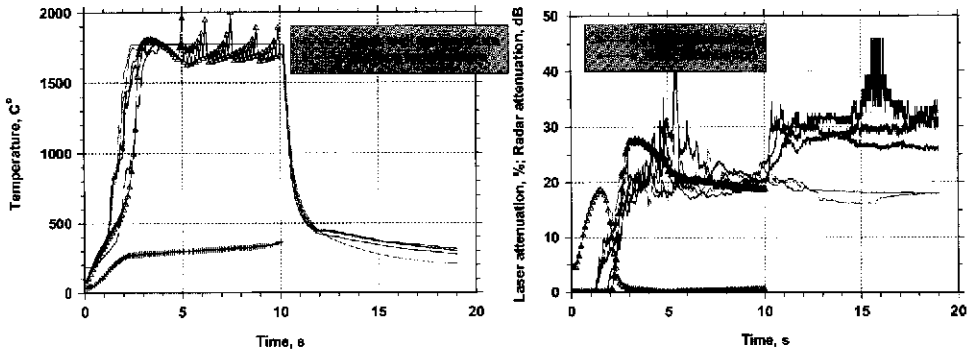

Fig. 6. Computed (symbols and lines) and measured[11] (lines) surface temperature and radar transmission for fiberglass for Nd:YAG laser (500 W/cm^2) interaction in airflow $M = 0.9$ with surface outgassing.

temporal behavior of surface temperature for 300 W/cm^2, reflecting the process of melting of glass fibers, agrees well with the experimentally measured data. The predicted depth of erosion after 10 s (Fig. 7) coincides exactly with the values measured by the authors with microcalipers: 0 mm for 175 W/cm^2, 2 mm for 300 W/cm^2, and 4 mm for 500 W/cm^2. The high-frequency excursions in temperature were associated with surface removal of material.

A feature of compelling interest in the radar attenuation measurements is the tendency for attenuation to decrease and/or to develop a plateau as time goes on. This tendency was observed for all power levels and a range of specimen thicknesses. Two mechanisms were examined numerically in an attempt to illuminate the physics behind these observations. For the first, we considered the physical removal of surface material by both chemical-reaction and thermal-stress-induced fracture. To produce constant attenuation, material must be removed at the same rate that attenuating char is formed. The removal mechanisms did produce the degree of removal observed at all power levels and also produced the falloff in attenuation at higher power levels. However, if removal rates were of magnitude equal to that of char formation, the model predicted specimen burn-through at the highest power

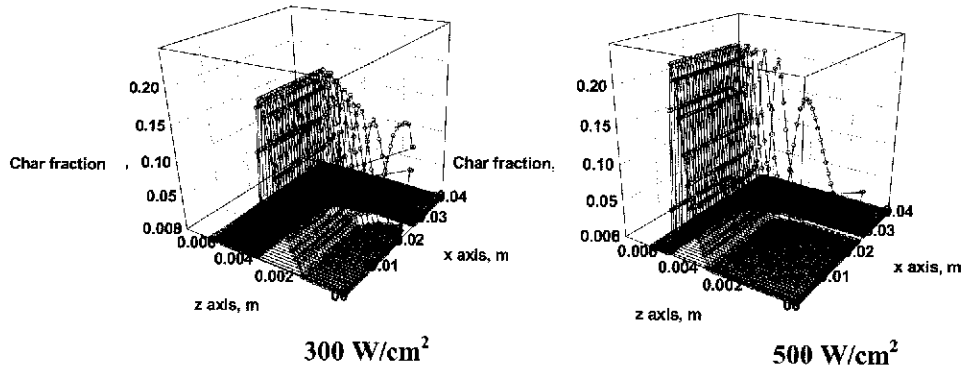

Fig. 7. Spatial distribution of the char volumetric fraction after 10 s of laser exposure with irradiance of 300 and 500 W/cm^2.

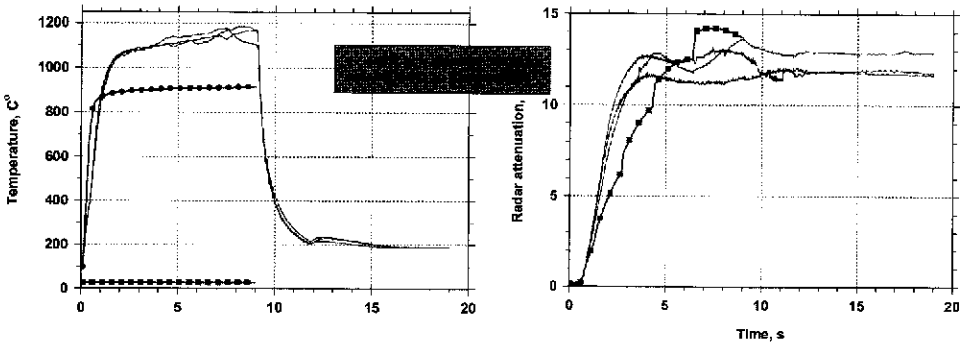

Fig. 8. Computed (symbols and lines) and measured[11] (lines) surface temperature and radar transmission for fiberglass for CO_2 laser interaction (175 W/cm^2) in airflow $M = 0.9$ with surface glass evaporation.

levels. Furthermore, if one considers that no char was removed at the lowest power level, one must conclude that this mechanism was not responsible for the low power attenuation plateau.

The second mechanism proposes that if cooling of the specimens is sufficient, then the temperature of the char farthest away from heating can be kept under the amorphous-to-crystalline transition point. Plotted in all of the Nd:YAG surface temperature figures are predictions of the back wall temperature. Note that while the back wall temperature initially increases rapidly, it transitions to almost a constant value at the same time that the radar attenuation plateaus. This is due to the finite area over which the specimen is irradiated. The cooled surface surrounding the irradiated area offers a path by which heat is conducted away from the underside of the char layer.

The predicted radar attenuation for the CO_2 laser irradiances of 175, 300, and 500 W/cm^2 are all in excellent agreement with the experimental measurements (as shown in Figs. 8–10). These figures also show that the predicted surface temperatures are also in excellent agreement, except for the case of beam irradiance of 175 W/cm^2, when the computed surface temperature is approximately 30% less than the measured temperature. The predicted temporal behavior of the surface temperature for the case of 300 W/cm^2 reflects the glass-melting

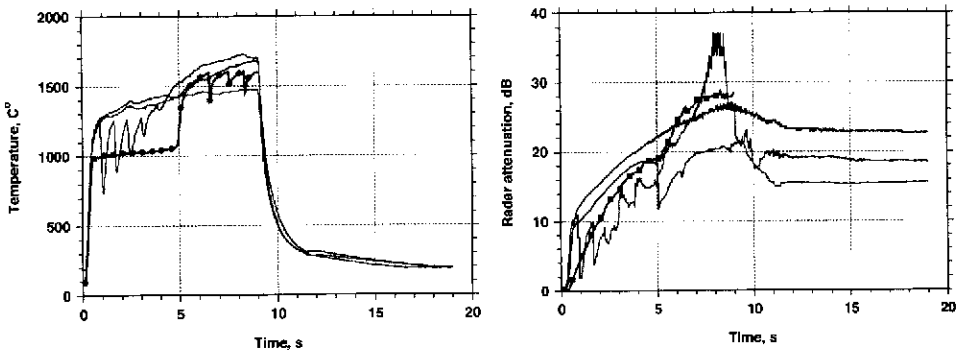

Fig. 9. Computed (symbols and lines) and measured[11] (lines) surface temperature and radar transmission for fiberglass for CO_2 laser interaction (300 W/cm^2) in airflow $M = 0.9$ with surface glass evaporation.

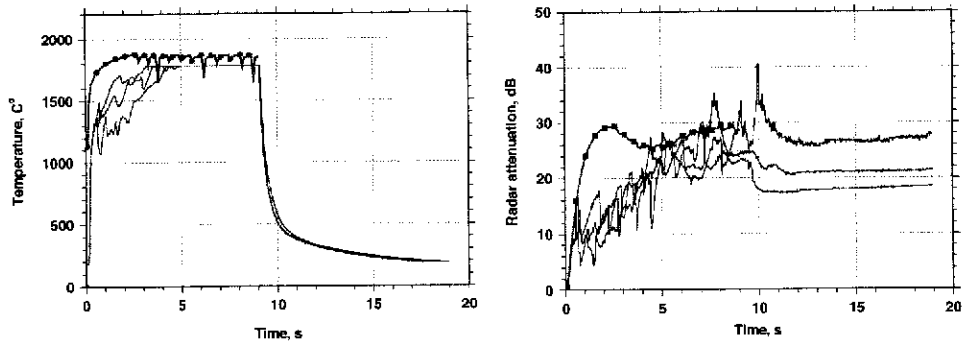

Fig. 10. Computed (symbols and lines) and measured[11] (lines) surface temperature and radar transmission for fiberglass for CO_2 laser interaction (500 W/cm^2) in airflow $M = 0.9$ with surface glass evaporation.

dynamics and matches the experimental data remarkably well. The much improved matching of model and experiment for the CO_2 laser case was attributed to the fact that the laser flux was absorbed at the surface of the specimen. As a consequence, the relatively high degree of potential uncertainty regarding the characterized behavior of the internal transmission behavior that complicated the Nd:YAG simulations was not present for the CO_2 simulations.

6. Conclusions

The numerical predictions of the surface temperatures, radar attenuation, laser beam attenuation, and material removal rates for the fiberglass composite were obtained for the laser beam irradiances in the range from 175 to 500 W/cm^2, for two wavelengths of 1.06 and 10.6 μm. A high degree of fidelity and consistency of the model predictions was seen in comparisons with the experimental measurements of laser transmission, surface temperature, and RF absorption. The model used a manageable number of empirically based parameters, which can be determined via relatively inexpensive testing. Barring the development

of accurate physics-based submodels for different fiberglass composites, limited measurements are required for different specimen materials. However, the qualitative dependencies of these parameters are modeled based on first principles and appear to produce reasonable results for conditions well outside their initial ranges.

The model has shown the capability of accurately representing important and subtly nuanced behavior, namely,

1. The location of the point and magnitude of maximum laser transmission
2. The peaking and falling off of radar attenuation (associated in part with loss of material)
3. The plateau in radar attenuation (associated in part with the transition in carbon form and change in electrical conductivity with temperature)
4. The proper amount of charred surface removal
5. The fluctuating character of the surface temperature and radar attenuation caused by char removal
6. The latent heat effects of the glass fiber material (as seen by the change in temperature profile curvature)

7. Acknowledgments

This material is based on work supported by the Naval Sea Systems Command, Program Office PMS405, under Contract N00024-02-D-6604, Delivery Order 0050, through the Electro-Optics Center, ARL-Penn State, Subcontract S02-2; the Program Manager was J. Thomas Schriempf.

References

[1]Clever, R.M., and V.E. Denny, J. Spacecraft Rockets **12**(9), 558 (1975).

[2]Crane, K.C.A., and J.R. Brown, J. Phys. D **14**, 2341 (1981).

[3]Dubois, M., P.W. Lorraine, R.J. Filkins, and T.E. Drake, Appl. Phys. Lett. **79**(12), 1813 (2001).

[4]Guencheva, V., E. Grantscharova, and I. Gutzow, Crystal. Res. Technol. **36**, 1411 (2001).

[5]Kawamura, R., and T. Nakajima, Trans. Japan Soc. Aero. Space Sci. **14**(25), 51 (1971).

[6]Lloyd, C.T., S.D. Jensen, and R.F. Cozzens, Polymeric Mat. Sci. Eng. **91**(Fall), U465 (2004).

[7]Mastanoiah, K., J. Heat Transfer **98**(Feb.), 139 (1976).

[8]McHenry, M.R., and B. Laub, Proc. SPIE **297**, 107 (1983).

[9]Mills, A.F., A.V. Gomez, and G. Strouhal, J. Spacecraft Rockets **8**(6), 613 (1971).

[10]Murray, A.L., and G.W. Russell, J. Spacecraft Rockets **39**(4), 501 (2002).

[11]Sames, D.J., "Experimental Effects of HEL for Radome Charring," DEPS High Energy Laser Lethality Conference, Newport News, VA, Sept. 2003.

[12]Scala, S.M., "The Hypersonic Ablation of Graphite," W.M. Rohsenow (ed.), in *Developments in Heat Transfer*, MIT Press, Cambridge, MA, 1964, Chap. 16, pp. 422–444 (1964).

[13]Scala, S.M., and L.M. Gilbert, ARS J. **32**, 917 (1962).

[14]Schlichting, H., *Boundary-Layer Theory*, 6th Ed., McGraw–Hill, pp. 647–648 (1968).

[15]Torre, L., J.M. Kenny, G. Boghetich, and A. Maffezzoli, J. Mat. Sci. **35**, 4563 (2000).

[16]Turns, S.R., *An Introduction to Combustion: Concepts and Applications*, McGraw–Hill (1996).

[17]"User's Manual: Aerotherm Charring Material Thermal Response and Ablation Program," Acurex Corp., Rept. UM-87-11/ATD, Mountain View, CA, Aug. 1987.

[18]Zhang, Z.J., K. Naruma, and H. Naramoto, J. Phys.: Condensed Matter **13**(22), L465 (2001).